Vol. 90 No. 2 pp. 440–455 ACTA GEOLOGICA SINICA (English Edition) Apr. 2016

Tectonic Imprints of the Hazara Kashmir Syntaxis on the Mesozoic Rocks Exposed in Munda, Mohmand Agency, Northwest Pakistan

Asghar ALI*, Umer HABIB, Atta Ur REHMAN, Noor ZADA,
Zain Ul ABIDIN and Muhammad ISMAIL

Department of Geology, University of Peshawar, Pakistan

Abstract: Two well-developed mesoscopic folds, D_2 and D_3, which postdate the middle amphibolite metamorphism, were recognized in the western hinterland zone of Pakistan. NW–SE trending D_2 folds developed during NE–SW horizontal bulk shortening followed by NE–SW trending D_3 folds, which developed during SE–NW shortening. Micro- to mesoscopically the NW–SE trending S_2 crenulation cleavage, boudins and mineral stretching lineations are overprinted by D_3. The newly established NW–SE trending micro- to mesoscopic structures in Munda termed D_2, which postdated F_1/F_2, is synchronously developed with F_3 structures in the western hinterland zone of Pakistan. We interpret that D_2 and D_3 folds are counterclockwise rotated in the tectonic event that has evolved the Hazara Kashmir Syntaxis after the main phase Indian plate and Kohistan Island Arc collision. Chlorite replacement by biotite in the main matrix crenulation cleavages indicates prograde metamorphism related with D_2. The inclusion of muscovite and biotite in garnet porphyroblasts and the presence of staurolite in these rocks indicate that the Barrovian metamorphic conditions predate D_2 and D_3. We interpret that garnet, staurolite and calcite porphyroblasts grew before D_2 because the well developed S_2 crenulation cleavage wraps around these porphyroblasts.

Key words: western hinterland zone, Hazara Kashmir Syntaxis, mesostructures, microstructures, metamorphism, tectonics

1 Introduction

The Kohistan Island Arc formed as a result of subduction of the Tethys oceanic lithosphere beneath the same plate in the Cretaceous. The Indian plate collided with the Kohistan Island Arc after consumption of the intervening Tethys Ocean (Khan et al., 2009; Faisal et al., 2014; Lu et al., 2015; Xu et al., 2015). Continued collision between these two blocks resulted in S-directed overthrusting of the Kohistan Island Arc onto the Indian passive continental margin along the Main Mantle Thrust (MMT; Tahirkheli et al., 1979; Coward et al., 1988). The MMT is strongly folded by the rapidly exhuming N–S trending Nanga Parbat anticline, for which monazite U/Pb ductile deformation ages range from 4 to 11 Ma and biotite cooling Ar/Ar ages range from 1 to 5 Ma (Smith et al., 1992; Schneider et al., 2001; Pecher et al., 2008). The western hinterland zone of Pakistan, which occupies the northwestern edge of the Indian plate, is metamorphosed to a granulite facies metamorphism. It is bounded to the north by the MMT, to the south by the Khairabad thrust and to the east by the Hazara Kashmir Syntaxis (HKS; Fig. 1). The western hinterland zone has undergone polyphase metamorphism and folding since collision of the Indian plate with the Kohistan Island Arc (Coward et al., 1986; Coward et al., 1988; Treloar et al., 1992; Anczkiewicz et al., 1998; DiPietro et al., 2008). As a whole this terrain is dominated by E–W trending macroscopic structures that are believed to have formed as a result of N–S shortening between the Indian Plate and the Kohistan Island Arc. The E–W trending structures in the western hinterland zone are deflected by tight to isoclinal HKS (Fig. 1; Burg et al., 2005). However, the tectonic imprints of the HKS on the rocks exposed in the western hinterland zone are poorly constrained. The metasedimentary rocks exposed in Munda, Mohmand Agency, northwest Pakistan preserve spectacular microscopic to mesoscopic structures and thus provide a unique opportunity to study the regional scale pre-, syn- and post-HKS imprints on these rocks. This study uses microscopic to mesoscopic structures including mineral

* Corresponding author. E-mail: asghar.ali@upesh.edu.pk

stretching lineations, intersection lineations, fold axes, axial plane foliations, fold vergence and boudins to understand the pre-, syn- and post-tectonic imprints of the HKS on the western hinterland zone of Pakistan.

2 Regional Geology

The composite Himalayan orogenic belt extends for over 2500 km from Afghanistan in the west to Burma in the east passing though Pakistan, India, China, Nepal and Bhutan. The Himalayan orogenic belt is divided into Higher (or Greater) Himalaya, Lower (or Lesser) Himalaya and Sub-Himalaya (Fig. 1). The Greater Himalaya forms the northern most part of the Indian plate, and contains Paleozoic to Mesozoic green schist to granulite facies metasediments, metavolcanic and igneous rocks underlain by Precambrian gneisses (Kearey and Vine, 1990). This unit is bounded to the north by the MMT/Indus suture (~61 Ma) and to the south the Khairabad Thrust overlies Precambrian to Mesozoic metasediments of the Lesser Himalaya (~20 Ma) (Fig. 1; Treloar et al., 1992; Pogue et al., 1999). Rocks of the Lesser Himalaya in the south thrust over Miocene terrigenous sediments of the Siwalik group along the Main Boundary Thrust (MBT; ~10 Ma) (Treloar et al., 1992). Progressive northward drift of the Indian plate plus the formation of these regional-scale thrusts have accommodated ~2000 km of crustal shortening (Pogue et al., 1999). The Precambrian to Mesozoic rocks exposed in the western hinterland zone have been deformed and metamorphosed multiple times. This regional scale metamorphism and deformation is strongly partitioned across the western hinterland zone. The central part is dominated by E–W trending structures while the western and eastern boundaries are dominated by NNW–SSE and NNE–SSW striking structures respectively. The southernmost E–W trending Khairabad, Panjal, Hissartang, Nathia Gali and MBT regional structures and Tertiary Siwalik series are tightly folded by the HKS (Fig. 2; cf. Bossart et al., 1988; Burg et al., 2005; Pecher et al., 2008). The overall structural geometry of these structures is counterclockwise rotated at

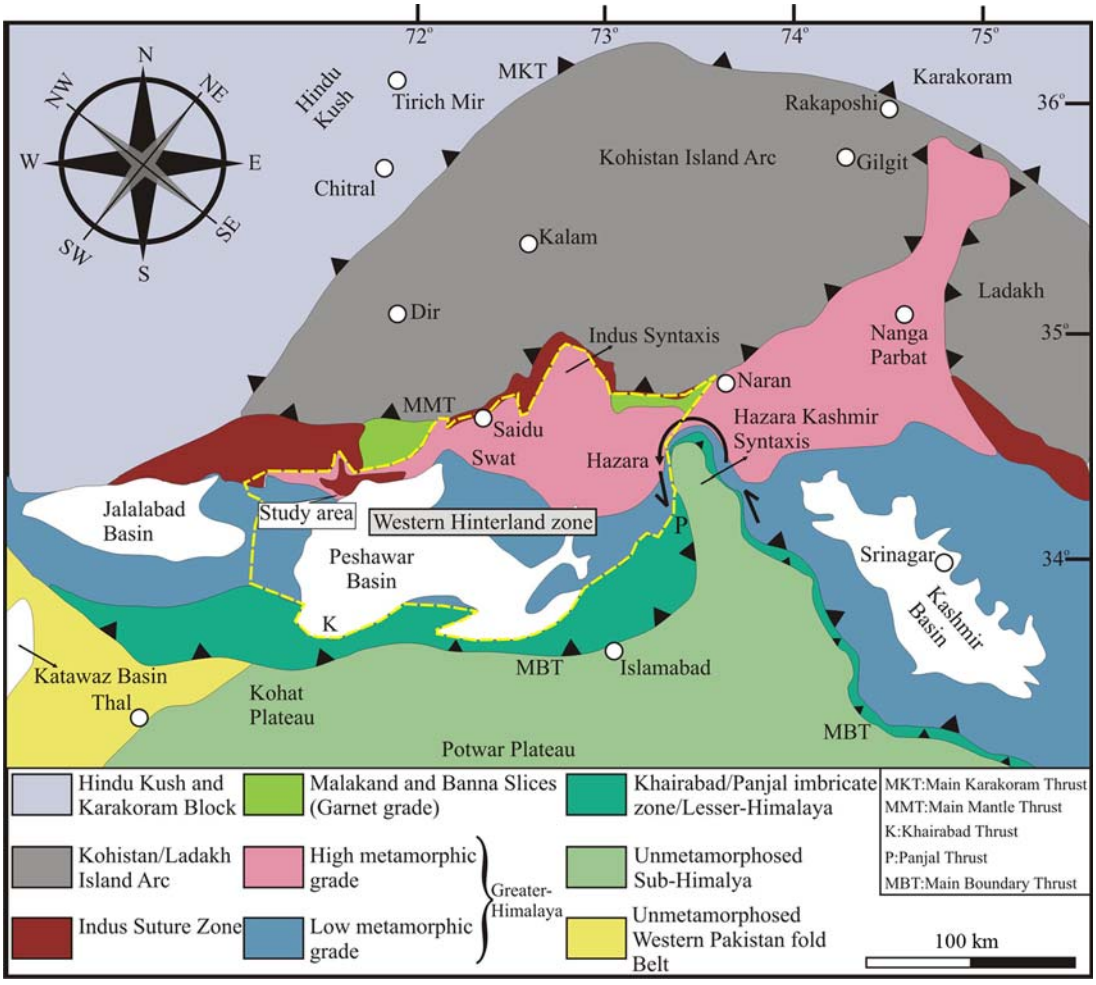

Fig. 1. Regional tectonic map of the HKS and the western hinterland zone of Pakistan. Note the Khairabad, Panjal and MBT faults are distinctly deflected with a sinistral shear sense in the apex region of the Syntaxis (after DiPietro et al., 2008).

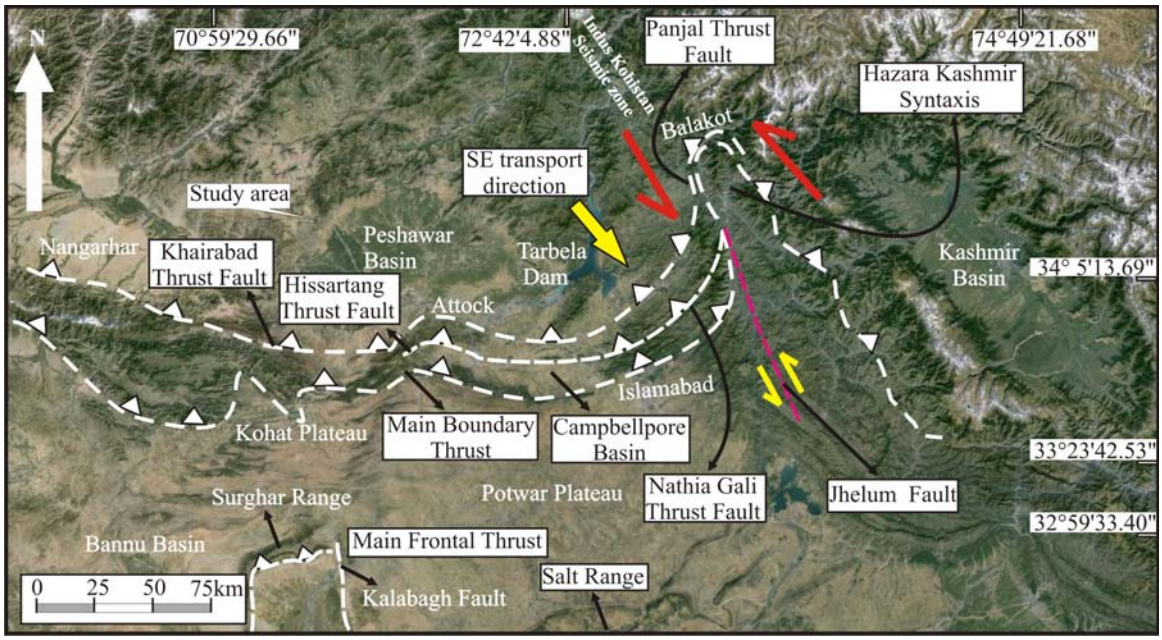

Fig. 2. Satellite map showing counterclockwise rotation of the regional Khairabad, Panjal, Nathia Gali Thrust Faults and MBT in the apex region of the KHS relative to the Indian plate with respect to true geographic north.

the apex of the HKS (cf. Bossart et al., 1988; Burg et al., 2005).

DiPietro et al., (2008) have reported four main phases, F_1/F_2, F_3 and F_4, of deformation in this region. Dominantly NW–SE trending F_1/F_2 deformation is tight to isoclinal outcrop-scale folds. These folds are infrequently observable mesoscopically as the younger deformation phases have obliterated them across the region. S_2 foliations, which are coeval with F_1/F_2, are penetrative with NW–SE, NE–SW and E–W trending mineral lineations. However, the NE–SW trending mineral stretching lineations are strongly dominant in the western hinterland zone (Fernandez, 1983). The metamorphism associated with this deformation is ~47 ± 3 Ma, as established from zircon rim overgrowth (Smith et al., 1994). F_1/F_2 early folds, and related foliations, are refolded by NW–SE to NE–SW trending F_3 open and upright folds in the Eocene (DiPietro and Lawrence, 1991). F_1/F_2 and F_3 are overprinted by E–W trending F_4 folds in the Oligocene (DiPietro and Lawrence, 1991). NNE–SSW shortening related to convergence of the Indian and Asian plates predates the Mio–Pliocene exhumation of the Nanga Parbat system, which occurred during WNW–ESE shortening. The HKS, which is exposed south of the Nanga Parbat, is characterized by ENE–WSW shortening.

The northern and northwestern parts of the western hinterland zone predominantly consist of the mutiply deformed and metamorphosed Precambrian to Early Mesozoic metasediments. The Cambrian to Lower Permian coarse grained granitic gneiss intruded the Precambrian Schist, which comprises tremolite marble and quartzo-feldspathic garnetiferous schist. These rocks are unconformably overlain by the Permian to Late Mesozoic multiply deformed and metamorphosed Alpurai group metasediments (Fig. 3). These rocks were metamorphosed under 575–685° C and 9 to 11.5 kbar metamorphic conditions in the northern and northwestern parts of the western hinterland zone. The Alpurai group metasediments are intruded by the unmetamorphosed Cenozoic Malakand granite. In the study area the Alpurai group metasediments are bound on the north by the MMT, on the south by the Peshawar Basin Quaternary alluvium, on the west by the undifferentiated Upper Proterozoic to Mesozoic rocks of the Khyber/Mohamand Agency and on the west by the mafic-ultramafic ophiolite complex of the Indus Suture Zone/ MMT (Fig. 3).

3 Detailed Petrographic Investigations

A total of 21 oriented samples were collected from the exposed Alpurai group metasediments in Munda (Fig. 3). Detailed petrographic investigations of 87 oriented thin sections from 21 samples indicate that the study area consists of middle amphibolite facies metamorphic rocks. These rocks comprise mainly quartz, calcite, chlorite, muscovite, biotite, garnet, graphite, plagioclase, staurolite and ilmenite. The well-developed matrix foliations are defined by well-oriented stretched quartz, elongated calcite, biotite, chlorite, muscovite and ilmenite (Fig. 4a). Elongated quartz grains in the main matrix foliation anastomoses around calcite, garnet, staurolite, biotite and

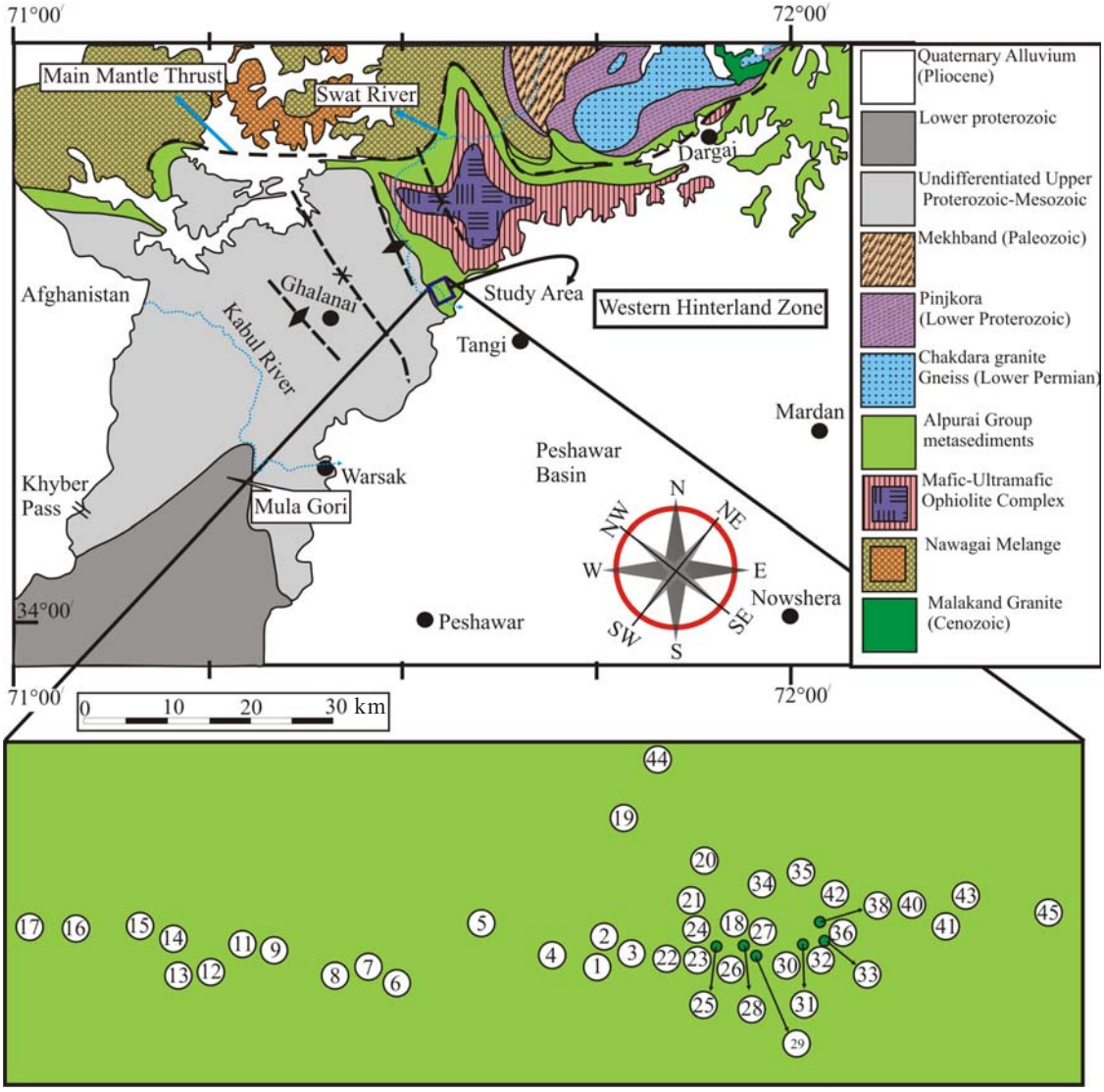

Fig. 3. Regional geological map showing location of study area located in the western hinterland zone, regional structural trends, sample locations and major stratigraphic units (modified after DiPietro et al., 2008).

recystallized coarse-grained undulose quartz. Quartz and calcite micro-boudins are also wrapped by elongated quartz grains (Fig. 4b). Calcite occurs as well-aligned elongated grains in the main matrix foliations and as twinned porphyroblasts in the microlithon/hinges (Fig. 4c, d). The well-defined S_2 matrix foliation anastomoses around calcite porphyroblasts. Strain shadows around calcite porphyroblasts are occupied by microcrystalline quartz and calcite grains. Calcite porphyroblasts contain muscovite and quartz inclusions, which indicate that calcite porphyroblasts postdated muscovite and quartz growth in these rocks. Chlorite, biotite and muscovite, which mainly define the main matrix foliations, were observed in crenulation and crenulated cleavages. Biotite displays perfect cleavage {001} and is aligned parallel to regional schistosity (Fig. 5a). The transformation of chlorite into biotite in the main matrix foliation designates prograde metamorphism across the region (Fig. 5b, c). Biotite porphyroblasts contain inclusions of ilmenite, which are arranged parallel to the same phase in the main matrix foliation (Fig. 5d). Elongated biotite aligned parallel the main matrix foliation nicely deflects around porphyroblasts and lenticular quartz micro-boudins. Muscovite predominantly occurs as well-aligned elongated flakes in the matrix foliations and less commonly as porphyroblasts. Sub-idiomorphic plagioclase poikiloblasts contain inclusions of biotite, quartz and muscovite. They are rimmed by muscovite and fine-grained quartz. The main matrix foliation anastomoses around plagioclase poikiloblasts. However, the highly altered plagioclase is oriented parallel to the main S_2 matrix foliations. Garnet porphyroblasts were observed in three samples. They contain sigmoidal inclusions of calcite, quartz, ilmenite, biotite and muscovite. The presence of biotite and

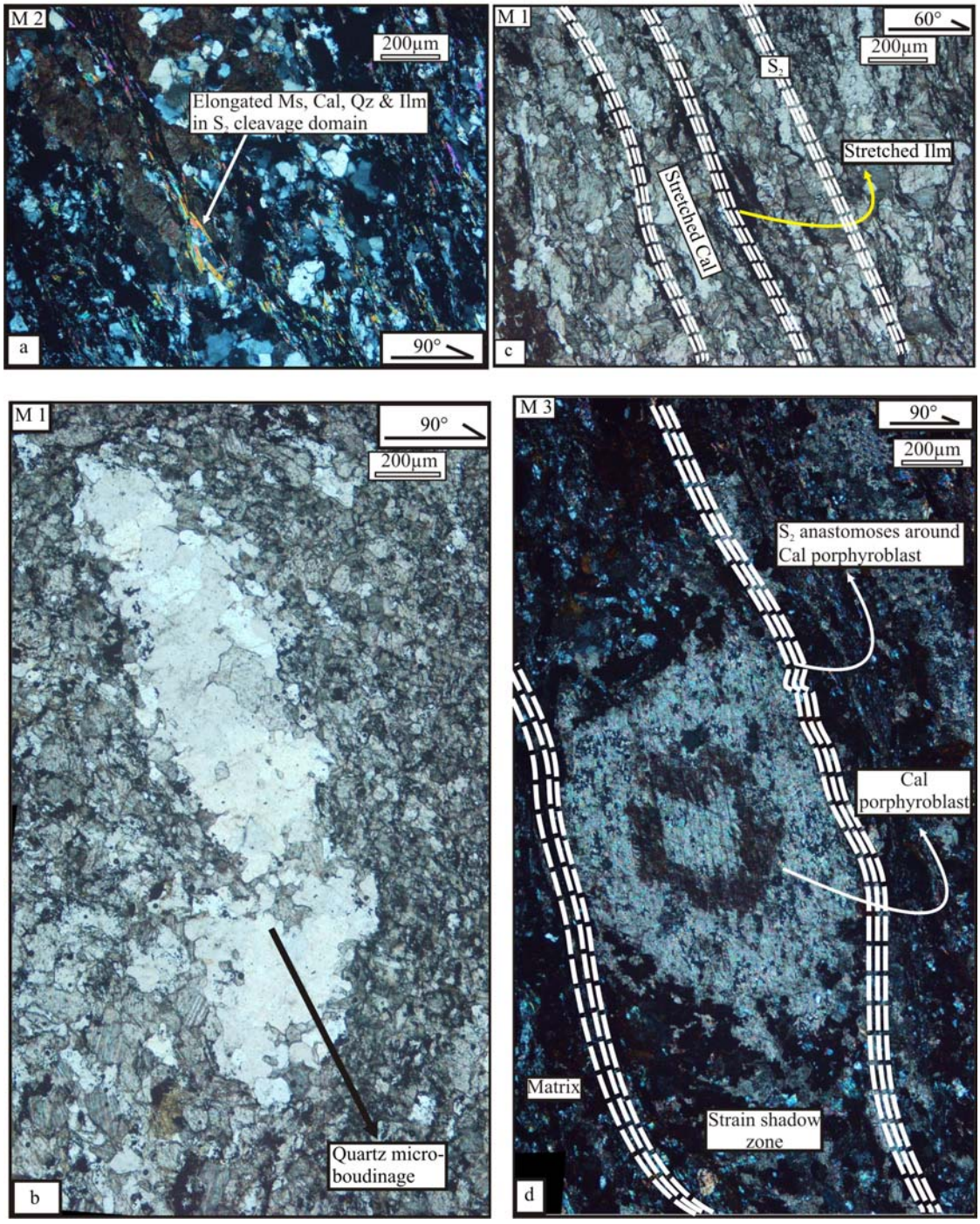

Fig. 4. Photomicrographs showing metamorphic mineral assemblages in the S_2 crenulation cleavages.
(a), Vertically oriented photomicrographs showing the concentration of elongated muscovite, quartz and calcite in the S_2 crenulation cleavage domain (XPL); (b), SSE pitching micro-boudinage is wrapped by elongated calcite and quartz grains (XPL); (c), Vertically oriented photomicrograph showing steeply pitching S_2 crenulation cleavages. The crenulation cleavages are defined by stretched calcite grains, ilmenite and muscovite (XPL); (d), Vertically oriented photomicrograph of SE steeply pitching S_2 crenulation cleavage, which anastomoses around the calcite porphyroblast. The calcite porphyroblast predates the S_2 crenulation cleavage in the matrix (Xpl). Mineral abbreviations are after Whitney and Evans (2010).

muscovite inclusions in garnet indicates that the later phase formed by reaction involving biotite and muscovite (cf. Whitney and Bozkurt, 2002). S_2 foliations deflect around garnet porphyroblasts (Fig. 6a). Staurolite porphyroblasts up to 1 mm in length and 200 μm across were observed in two samples, and the main matrix foliations anastomoses around staurolite. Quartz inclusion trails in staurolite are straight and truncated by S_2 in the matrix (Fig. 6b). The main matrix cleavage wraps around the staurolite, which provides evidence that they predated

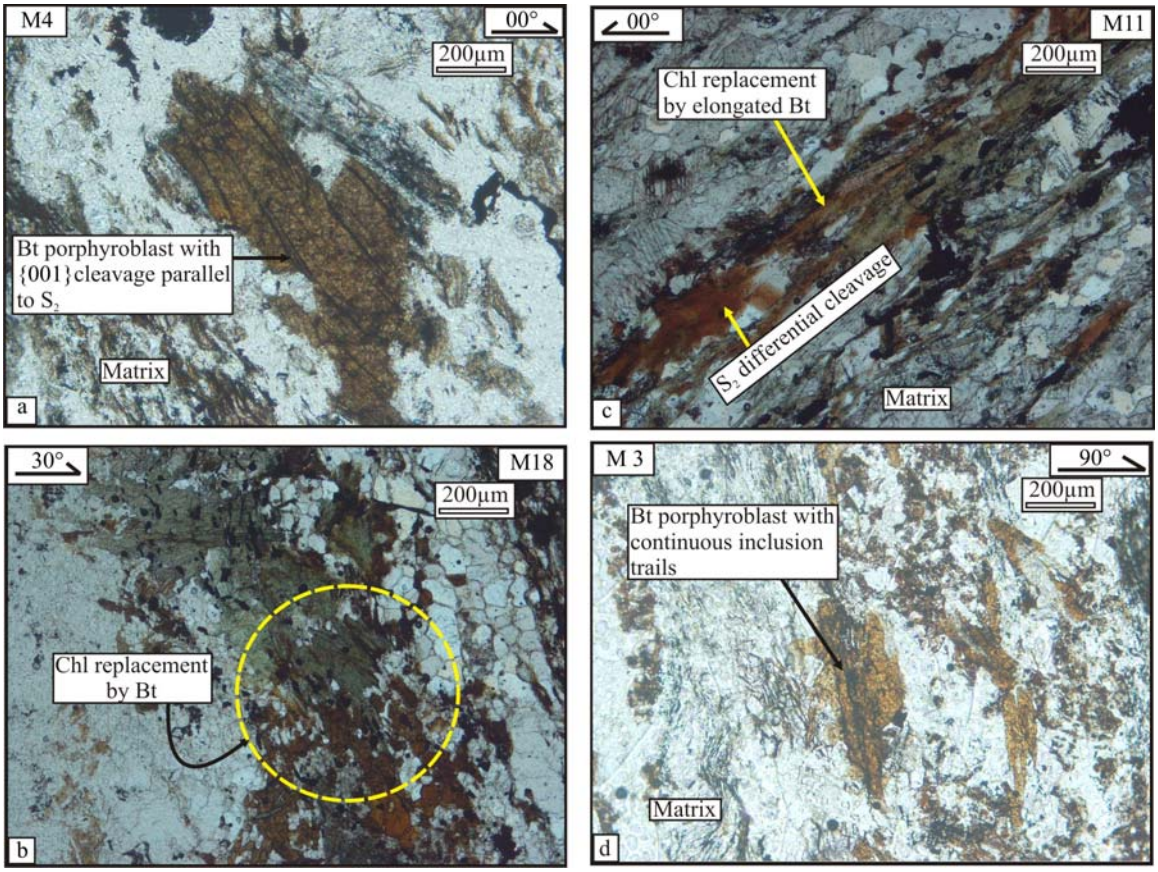

Fig. 5. Photomicrographs showing chlorite replacement by biotite in the S_2 crenulation cleavages.
(a), Vertically oriented photomicrograph showing biotite porphyroblast. The {001} cleavage of the biotite is parallel to S_2 crenulation cleavage. Note the matrix foliation does not wrap around the biotite porphyroblast, which indicates that they grew together during the same tectonic and metamorphic event (Ppl); (b), Photomicrograph illustrating chlorite replacement by biotite in the S_2 crenulation cleavage (Xpl); (c), Photomicrograph of vertical thin section showing the concentration of elongated biotite in the S_2 crenulation cleavage. Brownish elongated biotite replaces greenish elongated chlorite in the same cleavage. Biotite and chlorite along with elongated ilmenites arranged parallel to S_2 cleavage (Xpl); (d), Vertically oriented photomicrograph of biotite porphyroblast containing inclusion trails, which are continuous with the S_2 crenulation cleavage in the matrix (ppl). Mineral abbreviations are after Whitney and Evans (2010).

the S_2 tectonic event.

Microscopically S_1 crenulated cleavage is defined by z-shaped sigmoidal biotite, muscovite, quartz and ilmenite in the microlithon (Fig. 7a). Mesoscopically S_1 was observed in quartz and muscovite-rich, staurolite-bearing beds (Fig. 7b). D_2 parallel S_2 matrix foliations microscopically and mesoscopically are crenulated by D_3-induced S_3 crenulation cleavages (Fig. 8a, b; see below for details).

4 Mesoscopic Structures

Orogenic belts usually consist of superposed folding, which arises when the principal direction of bulk shortening changes during succeeding tectonic events (Ali, 2010; Sharib and Bell, 2011; Cao and Fletcher, 2012; Bell and Sapkota, 2012). The rocks of the western hinterland zone of Pakistan appear to have undergone multiple deformation and metamorphic events because microscopic to mesoscopic examination indicate three penetrative deformation events. These events were observed in the field, oriented horizontal slabs and thin sections (see supplementary data). Mesoscopically S_1 crenulations were observed in quartz and muscovite-rich, staurolite-bearing beds (Fig. 7b); elsewhere it is obliterated by D_2 and D_3 deformation events in the calcite- and mica-dominant units. Therefore the orientation of S_1 is not very well constrained in the study area. D_2 and D_3 are well preserved and observable at all scales. D_2 are close to tight NW–SE trending, gently NW plunging and slightly NW overturned mesoscopic folds (Fig. 9a–e). D_2 folds are prominently preserved in S_0 bedding in siliceous marble, quartzite and calcareous metapsammite beds. Moderately to steeply NE dipping axial plane cleavage strikes parallel to NW–SE trending D_2 fold axes and is continuous through succeeding folded layers. In rheologically different layers S_2 is highly penetrative and parallel to bedding S_0 at all scales of observation from microscopic to mesoscopic. Quartz-filled veins in the fairly homogeneous staurolite quartz mica schist display well developed ptygmatic folds. They have rounded hinges vs. straight limbs with

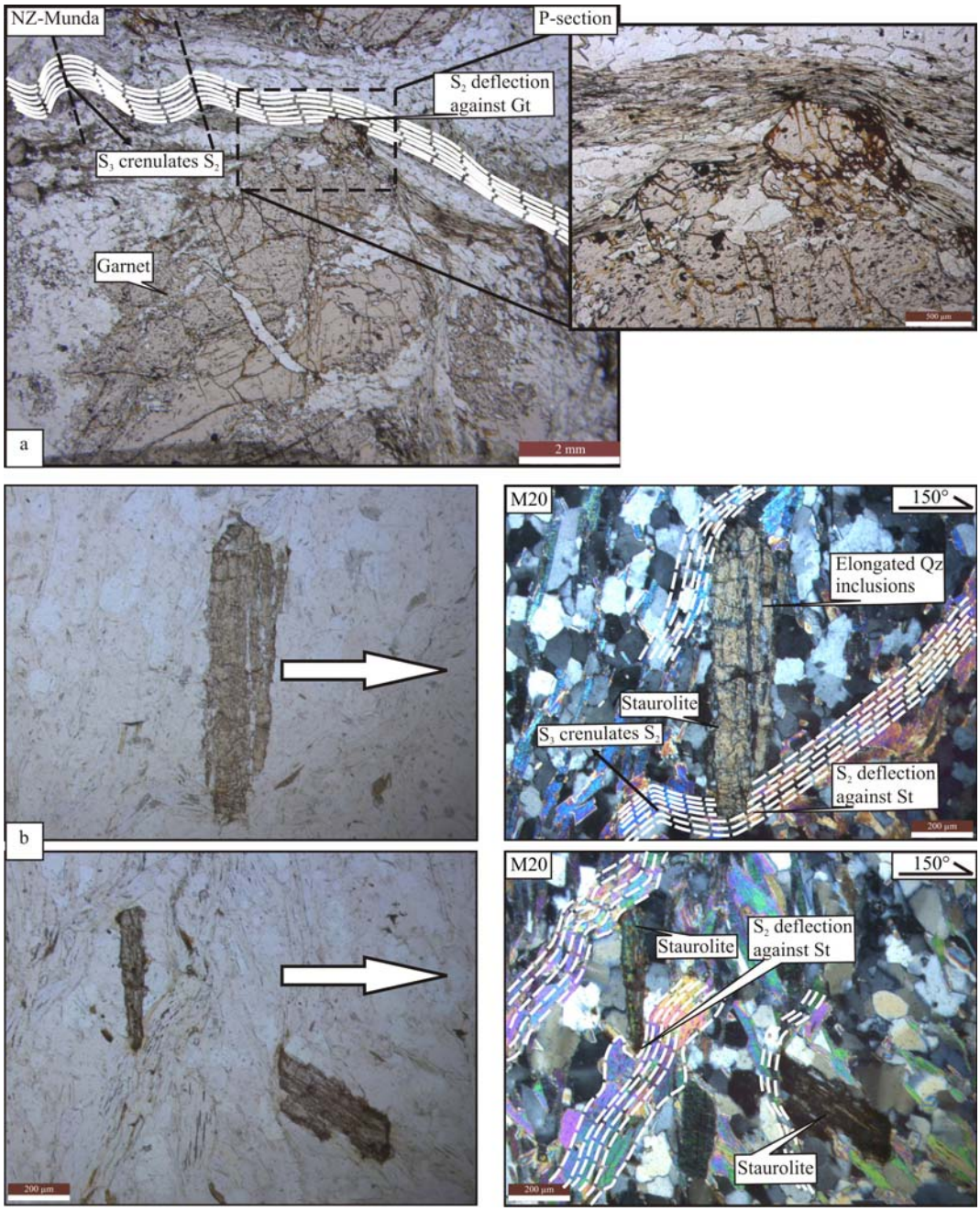

Fig. 6. Photomicrographs illustrating geochronologic relationship of garnet and staurolite porphyroblasts with the main matrix foliations.

(a), Photomicrograph of thin section cut parallel to regional schistosity showing well developed garnet porphyroblast. The main matrix foliation S_2 anastomoses around garnet porphyroblast (ppl); (b), Vertically oriented photomicrographs showing staurolite porphyroblasts. The main matrix foliations S_2 anastomoses around elongated staurolite porphyroblasts. Elongated quartz inclusion trails in staurolite are truncated by S_2 in the matrix.

amplitude higher than the wavelength. The fold axes of ptygmatic folds strike parallel to D_2 fold axes (Fig. 9f). Respectively a total of 66 dip and dip directions of S_2 foliations and 18 axial planes of mesoscopic folds were plotted on stereonets (Fig. 10a–b). S_2 cleavages are strongly developed in the metapelites that contain high concentrations of micaceous minerals and have obliterated the bedding. Foliation development in rocks is directly related to lithological differences between layers (Ramsay and Huber, 1983; Huston, 1990). The NE–SW horizontal bulk shortening event has strongly developed S_2 penetrative cleavage in the metapelite beds while it has developed NW–SE striking close to tight folds in the siliceous marble and metapsammite layers. Elongated recystallized quartz, calcite, biotite and muscovite are aligned parallel to D_2 fold axial plane foliations.

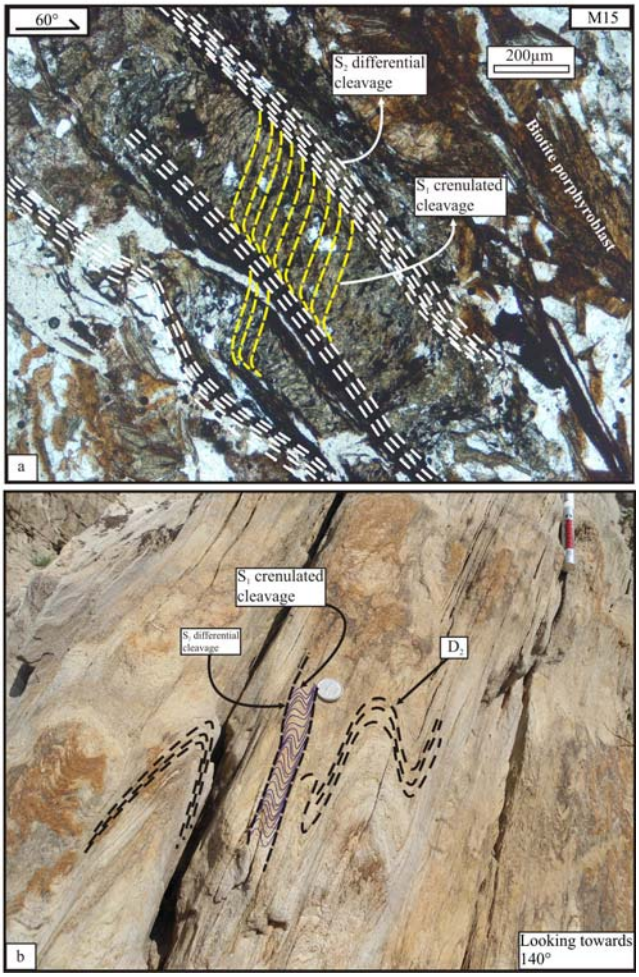

Fig. 7. Photomicrograph and fieldphotograph of the S_1 crenulated cleavage.
(a), Photomicrograph of a vertical thin section showing counterclockwise rotation of sigmoidal S_1 crenulated cleavage in the microlithon. The SE pitching S_2 crenulated cleavage is defined by elongated biotite and ilmenite (Ppl); (b), Oriented fieldphotograph showing S_1 crenulated cleavage preserved in quartz and muscovite rich, staurolite bearing bed.

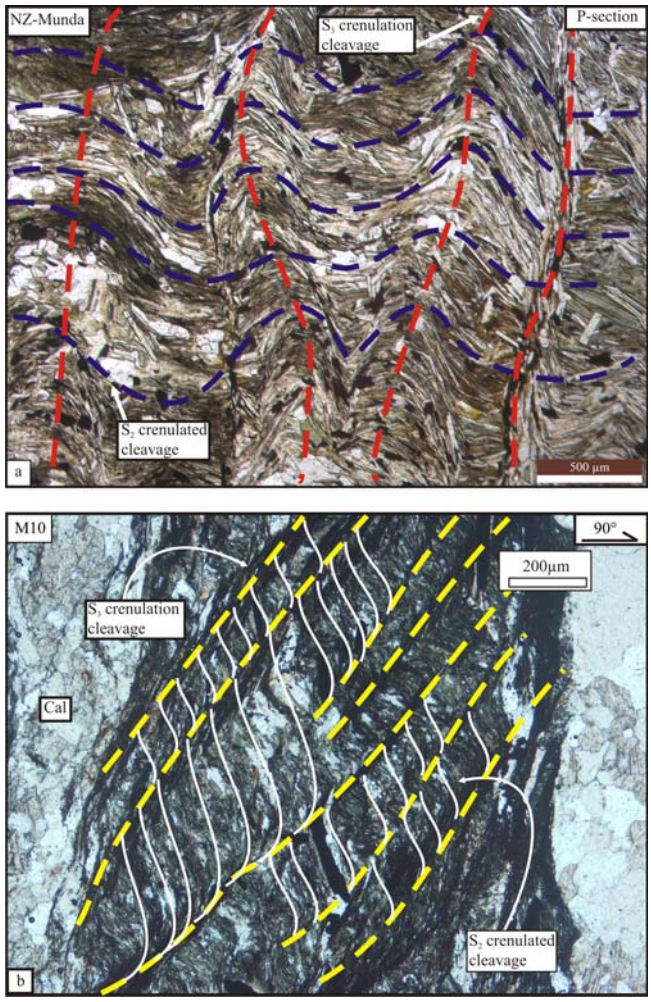

Fig. 8. Photomicrographs of the S_3 crenulation cleavages.
(a), Photomicrograph of thin section cut parallel to regional schistosity showing well developed S_3 crenulation cleavage. S_3, which developed during D_3 crenulates NW–SE trending S_2 crenulation cleavage across the region (ppl); (b), Oriented photomicrograph of a vertical thin section displaying relationship between D_2 and D_3 deformation events, NE–SW striking S_3 cleavage crenulates S_2 cleavage in the matrix (Xpl).

4.1 D_3 structures

Upright NE–SW trending D_3 open folds fold bedding parallel to S_2 in the region. The fold axes of these folds are moderately NE plunging while the NE–SW striking axial planes are nearly vertical. The plunge of D_3 is controlled by the dip amount of S_2 regional schistosity, which evolved during the D_2 deformation event. The amplitude of these folds is much smaller than D_2 folds. They are characterized by round hinges, while D_2 have sharp hinges and steeply dipping limbs. D_3 displays weakly developed axial plane foliations, which are hard to distinguish from the D_3 fold hinges. The quartz boudins and L^2_2 mineral lineations folded with variable plunge directions across D_3 fold hinges (Fig. 11). Microscopically S_3 is defined by crenulation of S_2 foliations. A total of eight measurements were made on the well-developed D_3 fold axes and their preferred orientations were plotted on a stereonet (Fig. 10d).

4.2 Lineations

Lineations are unidirectional structures that result from mineral elongation, boudins, intersection of two planes, crenulation axes, minor fold axes, elongated clasts, fault grooves and segregated veins (McClay, 1987). Study of lineation in multiply deformed terrains elucidates shortening and instantaneous elongation directions. Mineral stretching lineations in most cases develop in tectonites parallel to mesoscopic fold axes. However, during flexural folding mineral stretching lineation could remain perpendicular to the fold axis. It may form from stretching of existing minerals, fossils and pebbles or from crystallization of new minerals. The intersection lineations form from bedding-cleavage intersection or from

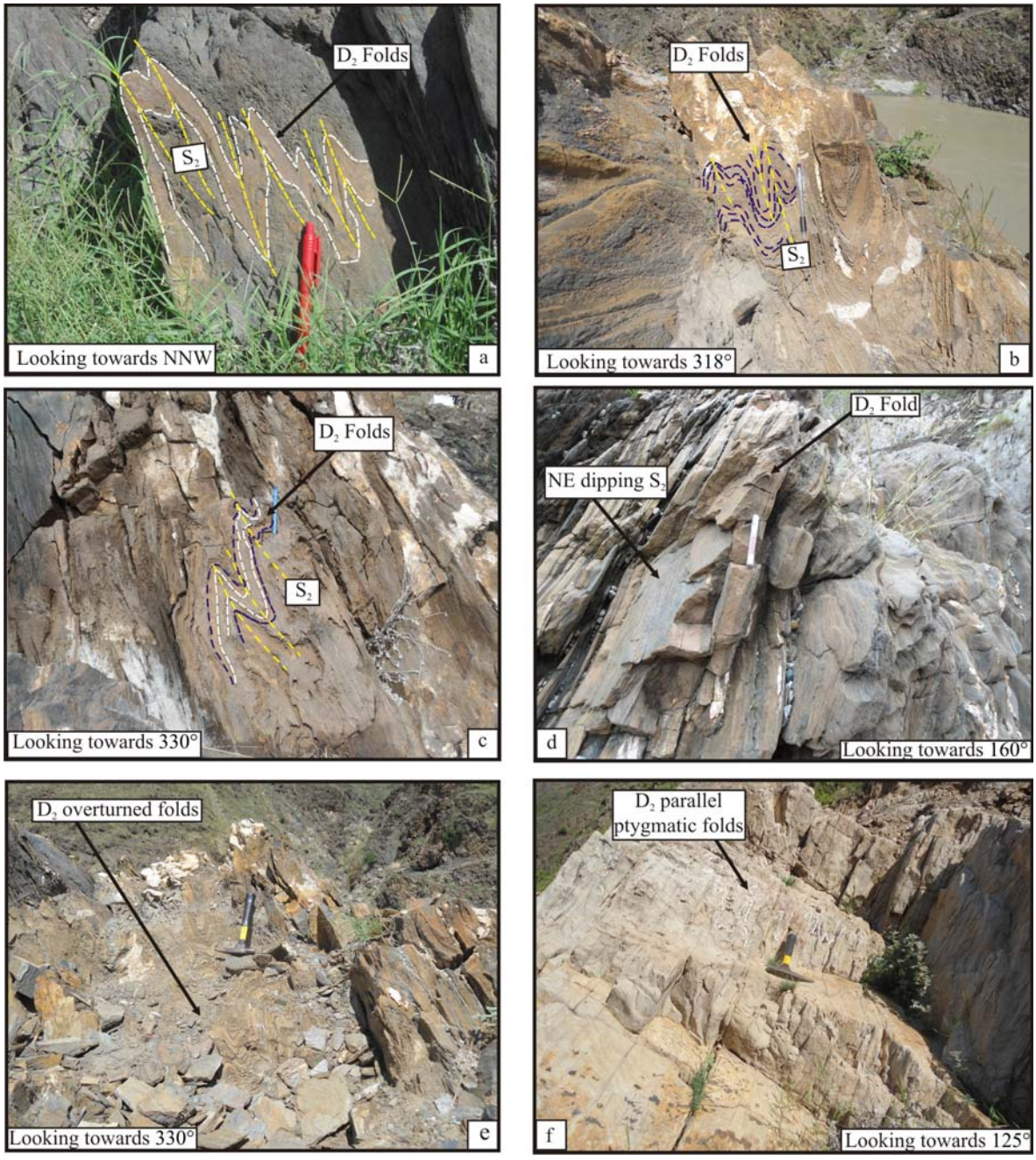

Fig. 9. Field-photographs of D_2 folds.
(a, b, c, d, e), Oriented field photographs showing NW–SE trending, NW gently plunging and slightly WNW overturned, mesoscopic close to tight D_2 folds and NE dipping S_2 axial plane foliations. D_2 folds are nicely preserved in places where the least competent pelitic schist surrounds the more competent quartzitic or psammitic beds; (f), Quartz filled veins in the fairly homogeneous staurolite quartz mica schist display well-developed ptygmatic folds. They have rounded hinges vs. straight limbs with amplitude higher than the wavelength.

cleavage-cleavage intersection. Cleavage-cleavage intersection lineation reflects more than one deformation event in a region. Intersection lineation remains parallel to the youngest deformational fold axes. Both mineral stretching and intersection lineation were measured at outcrop and from oriented photographs.

A competent layer or vein surrounded by less competent material segregates into boudin/lens structures during ductile deformation (Goscombe et al., 2004). In horizontal bulk shortening competent layers in a rock extend in the direction of the foliations; the gaps between the isolated segments fill by ductile flow of the surrounding less competent materials. Quartz veins parallel to bedding in the metapelitic schist are preferentially stretched in the direction of S_2 foliation at microscopic and mesoscopic scales (Figs. 4b, 12). The extension gaps between boudins are filled by the less competent metapelitic schist materials. A total of 230 measurements were made at

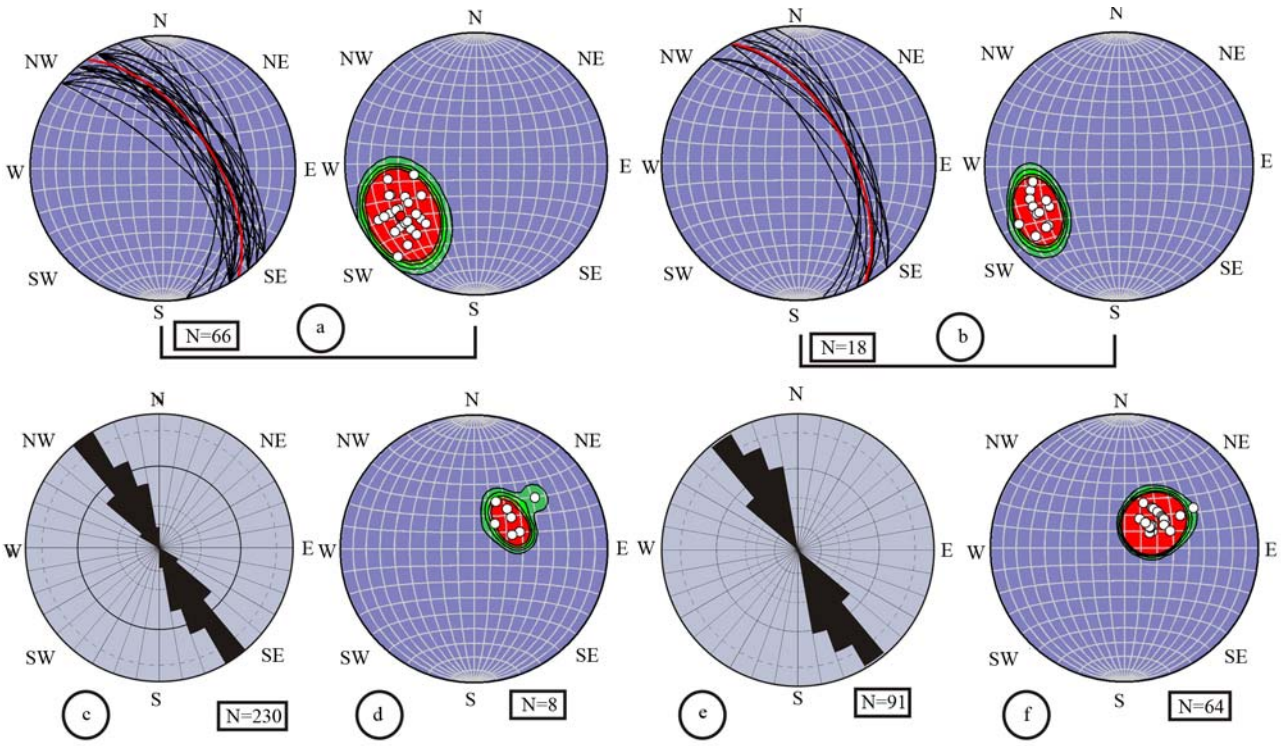

Fig. 10. Lower-hemisphere stereographic projections of mesoscopic structures.
(a), Lower-hemisphere equal area stereo-plots showing orientations of NW–SE trending S_2 foliations. The white dots represent poles to the great circles; (b), Lower-hemisphere equal area stereo-plots showing orientations of NNW–SSE trending and NE dipping D_2 axial planes. The white dots in the lower stereo-plot represent poles to the great circles; (c), Equal area rose diagram showing orientation of NW–SE trending segregated quartz boudins. These boudins are preferentially stretched in the direction of S_2 at both microscopic and mesoscopic scales; (d), Lower-hemisphere equal area stereo-plots poles of D_3 fold axes. D_3 fold axes are plunging towards NE. Note the total plunge of D_3 is controlled by S_2 dip; (e), Equal area rose diagram of L^2_2 mineral lineations. These mineral lineations are parallel to quartz boudins and S_2 axial plane foliations; (f), Lower-hemisphere equal area stereo-plots poles of L^3_2 intersection lineations and L^3_3 mineral lineation. Both lineations are plunging towards NE.

outcrop and from oriented photographs on stretched quartz boudins plotted on a stereonet (Fig. 10c). The neck zones of boudins are completely devoid of hydrothermal material precipitations due to the highly ductile nature of the least competent materials (cf. Goscombe et al., 2004).

A total of 91 L^2_2 mineral lineations trending NW–SE were measured and their preferred orientation was plotted on a stereonet (Fig. 10e). L^2_2 mineral elongation lineations and ellipsoidal quartz boudins are parallel to D_2 fold axes. Stretching lineations of opaque minerals were predominantly observed in quartzite beds whereas the pelitic beds are dominated by ellipsoidal quartz boudins. A total of 20 vertical thin sections were prepared at high angles to NW–SE trending mesoscopic folds to see the mineral elongation lineations at microscopic scale. The dominant penetrative axial planar cleavages contain NW–SE trending aligned mineral lineation of quartz, calcite, muscovite, ilmenite, biotite and micro-ellipsoidal quartz and calcite boudins.

A total of 64 L^3_2 intersection lineations and L^3_3 mineral lineations were measured and their trend plotted on a stereonet (Fig. 10f). L^3_2 intersection lineations, which trend parallel to D_3, are defined by weak crenulations of S_2 penetrative foliation looking down the plunge of D_3 folds at mesoscopic scale (Fig. 13).

4.3 Fold and cleavage vergence

Fold and cleavage vergence are important in multiply deformed orogenic belts because they indicate shear sense and direction of transport. Asymmetric folds are characterized by short forelimbs and long back limbs where the former dips steeper than the latter. Asymmetric Z (dextral) and S (sinistral) mesoscopic folds allow comprehension of the regional-scale macroscopic folds (McClay, 1987). Vergence direction of asymmetric folds may better be studied in profile section viewing the horizontal direction of movement in the hinge zone (cf. McClay, 1987). Top to NW sinistral shear sense vergence direction of D_2 mesoscopic folds in the study area was established by forelimb and back limb relationships (Fig. 14).

5 Interpretation and Discussion

Two well-developed mesoscopic folds, D_2 and D_3, were well established in the region. NW–SE trending D_2 and NE–SW trending D_3 folds developed during NE–SW and SE–NW horizontal bulk shortening respectively. NE–SW

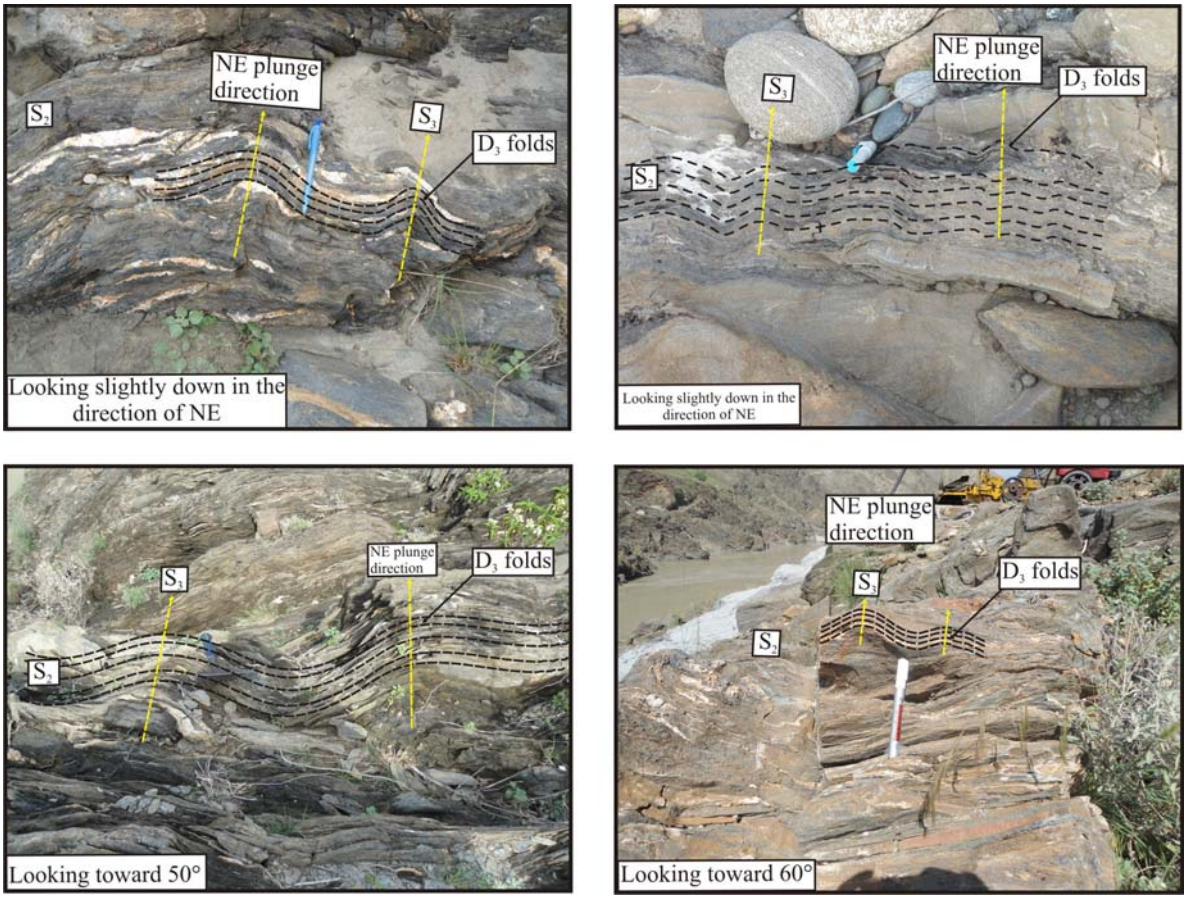

Fig. 11. Oriented photographs showing NE plunging D_3 folds, which crenulate well developed S_2 microscopically and mesoscopically. D_3 also folds NW–SE trending quartz boudins and L^2_2 mineral stretching lineations.

and NW–SE trending ~47±3 Ma F_1/F_2 that have been reported by DiPietro et al. (2008) in the western hinterland zone were not observed in these rocks. According to Ham and Bell (2004) in multiply and intensely deformed orogenic belts the reactivation of the compositional layering and bedding rotates the earlier foliations into parallelism with the younger deformation event. All the axial plane foliations in porphyroblasts and in strain shadows around competent bodies make successful correlation of older deformation and metamorphic events from outcrop to outcrop (Aerden, 2004; Bell, 2010; Bell and Sanislav, 2011). A very complex deformation history of the western hinterland zone is not preserved in these rocks due to the lack of porphyroblast growth during F_1/F_2, F_3 and F_4 deformation events. However, Yar (2013) reported deformation and metamorphic events preserved in multiply deformed metasedimentary rocks of the Silurian–Devonian Lowara Mena Formation, Mula Gori, ~32 km to the southwest of Munda (Fig. 3). In the Mula Gori region D_1, equivalent to F_1 of DiPietro et al. (2008), related foliations are preserved as inclusions in garnet cores and in garnets with truncated inclusion trails. Garnet containing continuous inclusion trails with the matrix preserved D_3, equivalent to F_4 of DiPietro et al. (2008). D_2, equivalent to F_3 of DiPietro et al. (2008), has no accompanying porphyroblast growth; these events have been established in the region from mesoscopic and microscopic matrix structures.

The growth of biotite porphyroblasts in Munda must have taken place during the D_2 deformation event because the straight inclusion trails preserved in this phase are continuous with the S_2 foliations in the matrix (Fig. 5d). Garnet, staurolite and calcite porphyroblasts grew before muscovite, biotite and chlorite in the axial plane foliations, as seen in the matrix foliations, which are exclusively defined by the later phases wrapped around the earlier

Table 1 Sequential growth of metamorphic index minerals in D_1, D_2 and D_3 deformation phases

Mineral Phase	Fold/Foliation Phase		
	D_1/S_1	D_2/S_2	D_3/S_3
Chlorite		Replace by biotite	
Muscovite			Crenulated by D_3
Biotite			Crenulated by D_3
Garnet		Anatomosed by S_2	
Staurolite		Anatomosed by S_2	
Plagioclase			Crenulated by D_3
Calcite			Crenulated by D_3

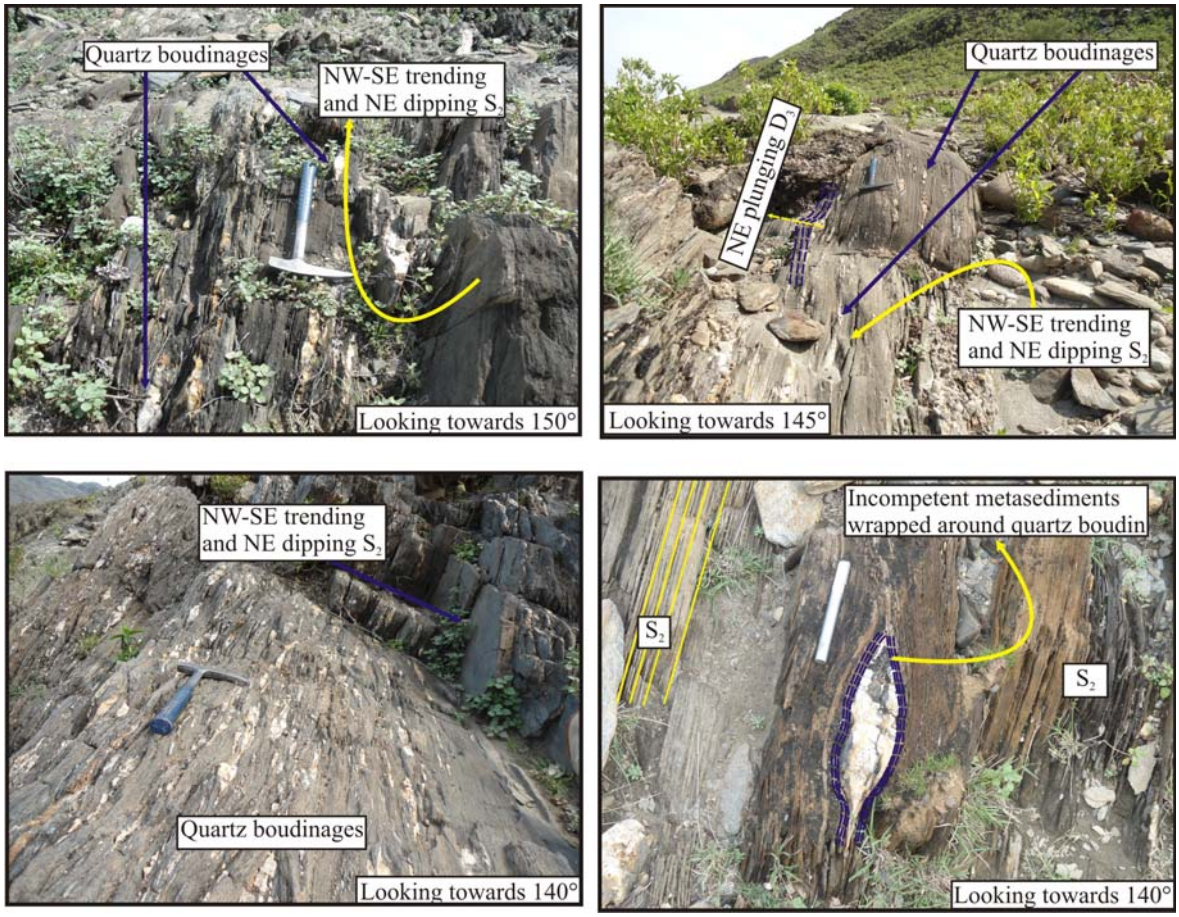

Fig. 12. Oriented field photographs showing NW–SE trending quartz boudins.
They are preferentially stretched in the direction of S_2. The extension gaps between individual boudins are filled by the least competent metapelitic schist material that followed during NE–SW horizontal bulk shortening associate with D_2 deformation event.

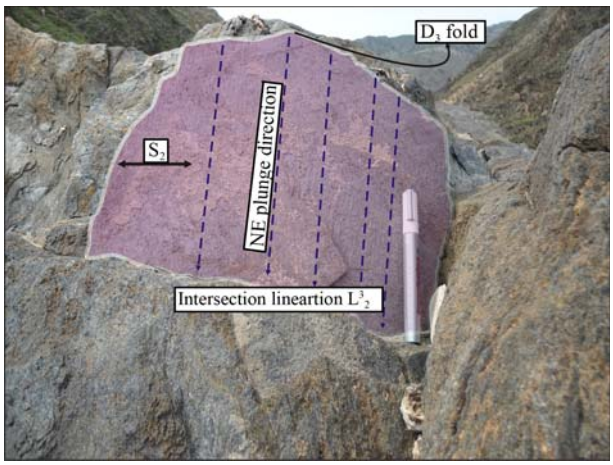

Fig. 13. Oriented photograph illustrating L^3_2 intersection lineation that developed from the intersection of S_2 and S_3 cleavages. The intersection lineations are trending in the direction of D_3 fold axes.

porphyroblasts (Table 1). D_2 folds in the region are followed by NE–SW trending D_3 upright open folds, which argue for SE–NW horizontal bulk shortening during the D_3 deformation event across the western hinterland zone. NW–SE trending S_2 cleavage, boudins and L^2_2 mineral stretching lineations are folded in the hinge zone of D_3 (Fig. 11). Microscopically the S_2 main matrix foliation defined by highly stretched quartz, muscovite, biotite and calcite is overprinted by S_3 (Fig. 8a–b). Samples containing NE–SW trending D_3 crenulation folds in the matrix foliations can properly be seen in thin section cut parallel to S_2 regional fabric (Fig. 8a). S_3 postdated S_2 and earlier biotite, muscovite, garnet, calcite, and staurolite growth in the region. D_3 folds were also identified in oriented horizontal slabs prepared from oriented samples; at hand specimen scale D_3 folds overprint main S_2 cleavage and NW–SE trending boudins (Fig. 15).

5.1 Tectonic significance

DiPietro and Lawrence, (1991) correlated the NW–SE trending F_1/F_2 and NW–SE to NE–SW striking F_3 folds in the Lower Swat to the trends of the Murree and Panjal thrust faults, which are exposed on the eastern side of the HKS (Fig. 1). This NNW–SSE trend of the HKS is completely different from all other exposed E–W structures in the west of the syntaxis. E–W trending

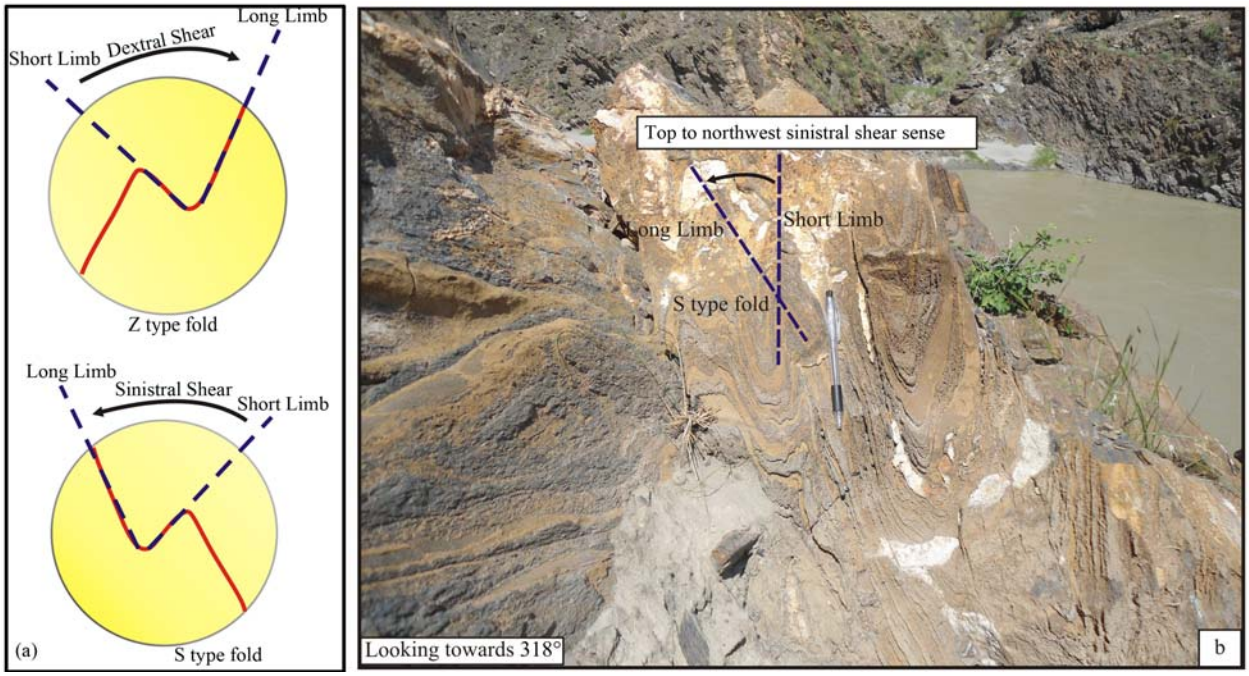

Fig. 14. (a, b), Schematic diagram and oriented photograph illustrating the method used for determination of vergence direction of D_2 mesoscopic folds. The vergence direction of mesoscopic folds in the study area was established by fore limb and back limb relationships.

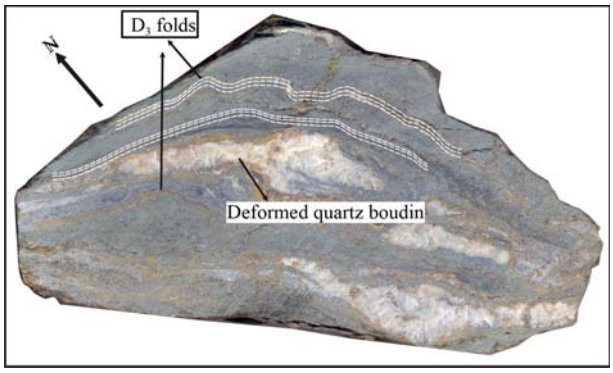

Fig. 15. Image of scanned horizontal slab showing D_3 mesoscopic folds. D_3 overprints S_2 axial plane foliation and NW–SE trending quartz boudins. D_3 fold is plunging towards NE.

Khairabad/Panjal, Hissartang/Nathia Gali and MBT regional thrust faults are tightly folded and distinctly deflected in a NW direction around the HKS (Figs. 1, 2; cf. Bossart et al., 1988; Burg et al., 2005; Pecher et al., 2008). A remarkably similar folding of the MMT in the Indus Syntaxis in Swat with a NNW–SSE trend and counterclockwise vergence appear to have formed synchronously with the HKS by the same changes in direction of bulk shortening in all of these regions (Fig. 1). Similarly, paleomagnetic studies of the Lower and Upper Tertiary molasse sediments on the western side of the HKS in the Attock Cherat Range, Potwar Basin and Salt Range also show counterclockwise rotation of these younger rocks relative to the Indian craton with respect to geographic north (Fig. 16). The NNW–SSE trending regional folds with NW vergence in Hazara Kashmir and Lower Swat suggests that they were linked orogenically and that a zone of comparable tectonism extended between these two regions. These NNW–SSE trending regional folds, which developed during ENE–WSW bulk shortening in both regions, overprint the south verging E–W tectonic grain of the western hinterland zone. Note that E–W trending structures in the western hinterland zone are equivalent to the F_4 macroscopic structures of Dipietero et al. (1991, 2008). The E–W trending F_4 associated structures in the western hinterland zone resulted from N–S shortening ~31 to 23 Ma ago. The subsequent N–S shortening between the Indian and Asian plates plus island arcs produced the E–W trending MBT about 10 Ma ago (Treloar et al., 1992). Along this regional boundary thrust, which extends from Pakistan to Nepal, the Jurassic unmetamorphosed rocks thrusted over the post-Eocene Siwalik Group clastic rocks. The MBT, along with the Khairabad, Hissartang and Natia Gali thrust faults, are tightly folded in the apex region of the HKS. Therefore, the HKS must postdate the NW–SE trending F_1/F_2 structures reported in the hinterland zone (DiPietro et al., 1991). The counterclockwise rotation of NW–SE structures in Munda termed D_2 both microscopically and mesoscopically post-dated the F_1/F_2, F_3 and F_4 structures. We interpret that D_2 overturning reflects the same tectonic

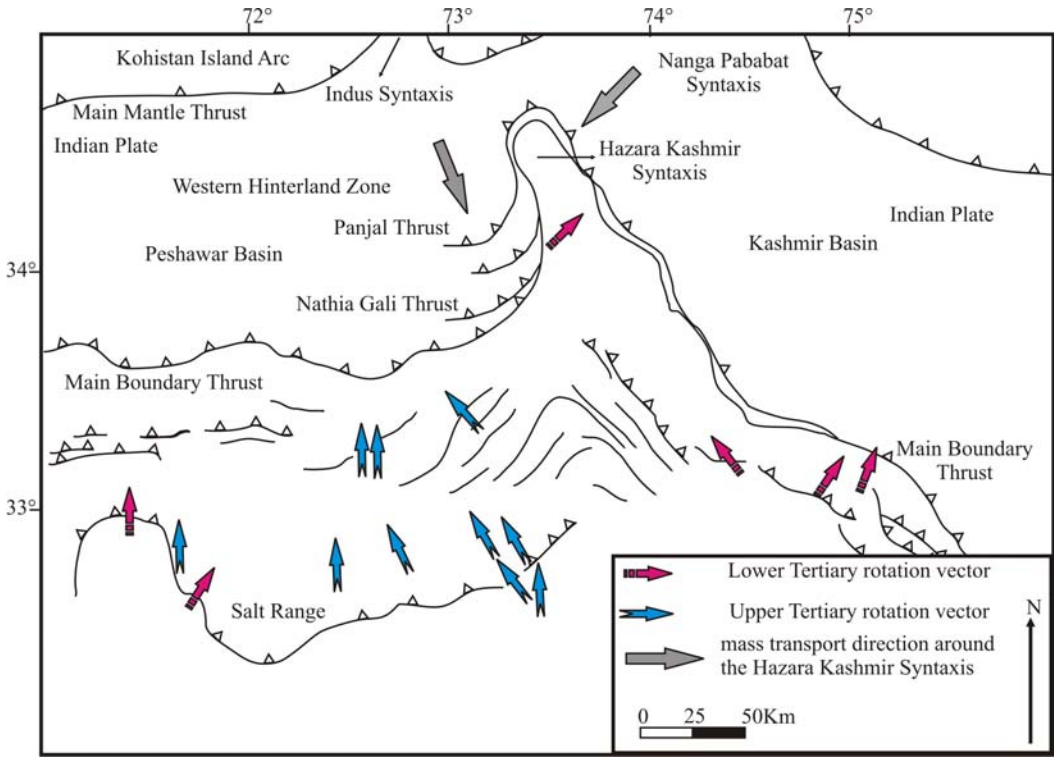

Fig. 16. Regional tectonic map of the hinterland zone, MMT and HKS showing counterclockwise rotation of the Lower and Upper Tertiary paleomagnetic vector and mass transport direction of the rocks exposed in the west of the HKS (after Bossart, 1989).

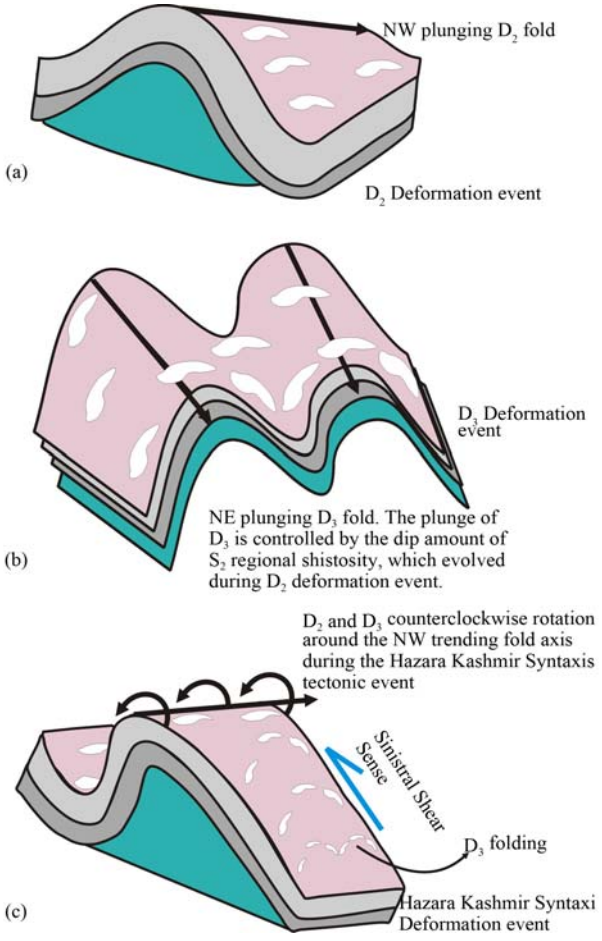

Fig. 17. Schematic diagram showing sequential imprints of D_3 and HKS on D_2. D_3 related folds did not rotate during the HKS tectonic event, because the NE limb of D_2, which contains D_3 folds transported top to NW around the D_2 fold axis.

event that produced the HKS in the Indian plate (Figs. 1–2). NW–SE trending axial plane cleavages and structures in the Munda region are overprinted by NE–SW trending folds that developed during SE–NW bulk shortening. D_3 predates the HKS counterclockwise rotation, as shown conceptually in Fig. 17. D_3-related folds did not rotate during the HKS tectonic event, because the NE limb of D_2, which contain D_3 folds, transported top to NW around the D_2 fold axis (Fig. 17).

Acknowledgements

We acknowledge financial support from the Department of Geology, University of Peshawar, and some logistical support and garnetiferous NZ samples from BAK Consulting Engineers. Ali appreciates the thin section preparation facilities provided by Department of Geology, University of Peshawar and petrographic facilities provided by the University of British Columbia, Canada and National Center of Excellence in Geology. I appreciate in-depth review of two anonymous reviewers and Fei Hongcai, Editor Acta Geologica Sinica.

Manuscript received Jan. 8, 2015
accepted Aug. 10, 2015
edited by Fei Hongcai and Kristian P. Saether

References

Aerden, D.G.A.M., 2004. Correlating deformation in Variscan NW–Iberia using porphyroblasts; implications for the Ibero–Armorican Arc. *Journal of Structural Geology,* 26: 177–196.

Ali, A., 2010. The tectono-metamorphic evolution of the Balcooma Metamorphic Group, north-eastern Australia: a multidisciplinary approach. *Journal of Metamorphic Geology,* 28: 397–422.

Anczkiewicz, R., Burg, J.P., Hussain, S.S., Dawood, H., Ghanzanfar, M., and Chaudhry, M.N., 1998. Stratigraphy and structure of the Indus suture in the Lower Swat, Pakistan: NW Himalaya. *Journal of Asian Earth Sciences,* 16: 225–238.

Bell, T.H., 2010. Deformation partitioning, foliation successions and their significance for orogenesis: hiding lengthy deformation histories in mylonites. In: Continental Tectonics and Mountain Building: The Legacy of Peach and Horne. Geological Society, London, Special Publications, 335. *Geological Society of London, Piccadilly*: 275–292.

Bell, T.H., and Sanislav, I.V., 2011. A deformation partitioning approach to resolving the sequence of fold events and the orientations in which they formed across multiply deformed large–scale regions. *Journal of Structural Geology*, 33: 1206–1217.

Bell, T.H., and Sapkota, J., 2012. Episodic gravitational collapse and migration of the mountain chain during orogenic roll-on in the Himalayas. *Journal of Metamorphic Geology*, 30: 651–666.

Bossart, P., Dietrich, D., Greco, A., Ottiger, R., and Ramsay, J.G., 1988. The tectonic structure of the Hazara Kashmir Syntaxis, Southern Himalaya Pakistan. *Tectonics,* 7: 273–297.

Bossart, P., Ottiger, R., and Heller, F., 1989. Paleomagnetism in the Hazara-Kashmir Syntaxis, NE Pakistan. *Eclogae Geologicae Helvetiae*, 82: 585–601.

Burg, P.J., Celerier, B., Chaudhry, M.N., Ghazanfar, M., Gnehm, F., and Schnellmann, M., 2005. Fault analysis and paleostress evolution in large strain regions: methodological and geological discussion of the southeastern Himalayan Fold-and-thrust belt in Pakistan. *Journal of Asian Earth Sciences,* 24: 445–467.

Cao, H., and Fletcher, C., 2012. FIA trends along the Precambrian Rocky Mountains: a new approach to timing continental docking. *Journal of Metamorphic Geology*, 30: 639–650.

Coward, M.P., Windley, B.F., Broughton, R.D., Luff, I.W., Petterson, M.G., Pudsey, C.J., Rex, D.C., and Khan, M.A., 1986. Collision tectonics in the NW Himalaya. In: Coward, M.P., and Ries, A.C. (eds.), *Collision Tectonics*. Geological Society Special Publication, 19: 203–219.

Coward, M.P., Butler, R.W.H., Chambers, A.F., Graham, R.H., Izatt, C.N., Khan, M.A., Knipe, R.J., Prior, D.J., Treloar, P.J., and Williams, M.P., 1988. Folding and imbrications of the Indian crust during Himalayan collision. *Philosophical Transactions of the Roval Society of London*, 326: 89–166.

DiPietro, J.A., and Lawrence, R.D., 1991. Himalayan structure and metamorphism south of the Main Mantle Thrust, Lower Swat, Pakistan. *Journal of metamorphic Geology*, 9: 481–495.

DiPietro, J.A., Ahmad, I., and Hussain, A., 2008. Cenozoic Kinematic history of the Kohistan fault in the Pakistan Himalaya. *Geological Society of American Bulletin*, 120: 1428–1440.

Faisal, S., Larson, P.K., Cottle, M.J., and Lamming, J., 2014. Building the Hindu Kush: monazite records of terrane accretion, plutonism and the evolution of the Himalaya Karakoram–Tibet orogen. *Terra Nova,* 26: 395–401.

Fernandez, A., 1983. Strain analysis of typical granite of the Lesser Himalayan cordierite granite belt: The Mansehra pluton, northern Pakistan. In: Shams, F.A., (ed.), *Granites of the Himalayas, Karakoram, and Hindu Kush*. Lahore, Institute of Geology, Punjab University: 183–200.

Goscombe, B.D., Passchier, C.W., and Hand, M., 2004. Boudinage classification: end member boudin types and modified boudin structures. *Journal of Structural Geology,* 26: 739–763.

Ham, A.P., and Bell, T.H., 2004. Recycling of foliations during folding. *Journal of Structural Geology* 26: 1989–2009.

Huston, D.L., 1990. The stratigraphic and structural setting of the Balcooma volcanogenic massive sulphide lenses, north Queensland. *Australian Journal of Earth Sciences,* 37: 423–440.

Kearey, P., and Vine, J.F., 1990. Global Tectonics. *Blackwell Scientific Publication*: 1–302.

Khan, S.D., Walker, D.J., Hall, S.A., Burke, K.C., Shah, M.T., and Stockli, L., 2009. Did the Kohistan-Ladakh island arc collide first with India? *Geological Society of America*, 121: 366–384.

Lu, L., Zhen, Z., Zhenhan, W., Cheng, Q. and Peisheng, Y. 2015). Fission Track Thermochronology Evidence for the Cretaceous and Paleogene Tectonic Event of Nyainrong Microcontinent, Tibet. *Acta Geologica Sinica* (English Edition), 89(1): 133–144.

McClay, K., 1987. The mapping of geological structures. Geological society of London handbook. Berkshire: Open University Press.

Pogue, K.R., Hylland ,M.D., Yeats, R.S., Khattak, W.U., and Hussain, A., 1999. Stratigraphic and structural framework of Himalayan foothills, Northern Pakistan. In: Macfarlane, A., Sorkhabi, R. B. and Quade, J., (eds.), Himalaya and Tibet: Mountain roots to Mountain tops: Boulder, Colorado. *Geological Society of America, Special paper*, 328: 257–274.

Schneider, D.A., Zeitler, P.K., Kidd, W.S.F., and Edwards, M.A., 2001. Geochronologic constraints on the tectonic evolution and exhumation of Nanga Parbat, western Himalaya syntaxis, revisited. *The Journal of Geology,* 109: 563–583.

Sharib, A.S.A.A.A., and Bell, T.H., 2011. Radical changes in bulk shortening directions during orogenesis: Significance for progressive development of regional folds and thrusts. *Precambrian Research*, 188: 1–20.

Smith, H.A., Chamberlain, C.P., and Zeitler, P.K., 1992. Documentation of Neogene regional metamorphism in the Himalayas of Pakistan using U-Pb in monazite. *Earth and Planetary Science Letters*, 113: 93 – 105.

Smith, H.A., Chamberlain, C.P., and Zeitler, P.K., 1994. Timing and duration of Himalayan metamorphism within the Indian plate, northwest Himalaya, Pakistan. *The Journal of Geology* 102: 493–508.

Ramsay, J.G., and Huber, M.I., 1983. *The techniques of modern structural geology, 1: Strain Analysis*. London: Academic

Press.

Tahirkheli, R.A.K, Mattauer, M., Proust, F., and Tapponnier, P., 1979. The India-Eurasia suture zone in northern Pakistan; synthesis and interpretation of recent data at plate scale. In: Farah, A., and De Jong, K.A. (eds.), *Geodynamics of Pakistan*. Geological Survey of Pakistan, Quetta: 125–130.

Treloar, P.J., Coward, M.P., Chambers, A.F., Izzat, C.N., and Jackson, K.C, 1992. Thrust geometries, Interferences and rotations in the North West Himalaya, In: McClay, K.R., (ed.), *Thrust Tectonic*s. Chapman and Hall, New York: 325–342.

Whitney, D.L., and Bozkurt, E., 2002. Metamorphic history of the southern Menderes massif, western Turkey. *Geological Society of America*, 114: 829–83.

Whitney, D.L., Evans, W.B., 2010. Abbreviations for names of rock-forming minerals. *American Mineralogist,* 95:185–187.

Xu, Z., Dilek, Y., Yang, J., Liang, F., Liu, F., BA, D., Cai, Z., LI, G. and Dong, H. 2015. Crustal Structure of the Indus-Tsangpo Suture Zone and its Ophiolites, Southern Tibet. *Acta Geologica Sinica* (English Edition), 89(z2): 103.

Yar, M., 2013. *Tectono-metamorphic evolution of Mula Gori area, Khyber Agency, NW Pakistan*. National Centre of Excellence in Geology, University of Peshawar: 79pp.

About the first author

Asghar ALI is working as Assistant Professor at the Department Of Geology, University Of Peshawar. He has a PhD from the James Cook University, Australia and postdoctoral fellowship at the University Of British Columbia, Canada. He obtained his B.Sc (Hons) and M.Sc degrees from the University Of Peshawar. Ali research interests are in structural geology (micro-scale to macro-scale structures associated with cyclic orogenic events), petrology, geochronology, thermodynamics and regional/global tectonics. He is concerned in applications of structures at all scale of observations to understand a very complex history of multiply deformed rocks in orogenic belts. He has published papers on tectonics and petrology.